

# A Layer-by-Layer Assembly Route to Electroplated Fibril-Based 3D Porous Current Collectors for Energy Storage Devices

Seunghui Woo, Donghyeon Nam, Woojae Chang, Younji Ko, Seokmin Lee, Yongkwon Song, Bongjun Yeom, Jun Hyuk Moon, Seung Woo Lee,\* and Jinhan Cho\*

Electrical conductivity, mechanical flexibility, and large electroactive surface areas are the most important factors in determining the performance of various flexible electrodes in energy storage devices. Herein, a layer-by-layer (LbL) assembly-induced metal electrodeposition approach is introduced to prepare a variety of highly porous 3D-current collectors with high flexibility, metallic conductivity, and large surface area. In this study, a few metal nanoparticle (NP) layers are LbL-assembled onto insulating paper for the preparation of conductive paper. Subsequent Ni electroplating of the metal NP-coated substrates reduces the sheet resistance from  $\approx 10^3$  to  $< 0.1 \Omega \text{ sq}^{-1}$  while maintaining the porous structure of the pristine paper. Particularly, this approach is completely compatible with commercial electroplating processes, and thus can be directly extended to electroplating applications using a variety of other metals in addition to Ni. After depositing high-energy MnO NPs onto Ni-electroplated papers, the areal capacitance increases from 68 to 811  $\text{mF cm}^{-2}$  as the mass loading of MnO NPs increases from 0.16 to 4.31  $\text{mg cm}^{-2}$ . When metal NPs are periodically LbL-assembled with the MnO NPs, the areal capacitance increases to 1710  $\text{mF cm}^{-2}$ .

## 1. Introduction

The rapid evolution of flexible and wearable electronics has attracted substantial interest in the development of energy

S. Woo, D. Nam, W. Chang, Y. Ko, S. Lee, Y. Song, Prof. J. Cho  
Department of Chemical and Biological Engineering  
Korea University  
145 Anam-ro, Seongbuk-gu, Seoul 02841, Republic of Korea  
E-mail: jinhan71@korea.ac.kr

Prof. B. Yeom  
Department of Chemical Engineering  
Hanyang University  
222 Wangsimni-ro, Seongdong-gu, Seoul 04763, Republic of Korea

Prof. J. H. Moon  
Department of Chemical and Biomolecular Engineering  
Sogang University  
Baekbeom-ro 35, Mapo-gu, Seoul 04107, Republic of Korea

Prof. S. W. Lee  
The George W. Woodruff School of Mechanical Engineering  
Georgia Institute of Technology  
North Ave NW, Atlanta, Georgia 30332, USA  
E-mail: seung.lee@gatech.edu

Prof. J. Cho  
KU-KIST Graduate School of Converging Science and Technology  
Korea University  
145 Anam-ro, Seongbuk-gu, Seoul 02841, Republic of Korea

 The ORCID identification number(s) for the author(s) of this article can be found under <https://doi.org/10.1002/smll.202007579>.

DOI: 10.1002/smll.202007579

storage electrodes with both high energy/power densities and mechanical flexibility.<sup>[1–18]</sup> In general, flexibility of the electrode can be achieved with a thin active layer on a 2D flexible current collector.<sup>[1–4]</sup> However, this electrode has much difficulty in significantly increasing the thickness of the active layer for enhancing its areal energy density because the thickly coated active layer can be easily delaminated from the 2D current collector under external stresses.<sup>[9]</sup> As a result, the reported electrodes have imposed a limit on increasing their areal energy density (i.e., energy density per unit area). Therefore, numerous approaches have focused on preparing 3D current collectors with large surface areas and mechanical flexibility that allow the incorporation of large amounts of electroactive electrode materials.<sup>[5–29]</sup> In particular, flexible paper and textile materials have emerged as

promising substrates for 3D current collectors due to their high surface areas, low cost, and excellent mechanical properties.<sup>[5–8,12,13,16–22]</sup> However, in order for these insulating substrates to be used as 3D current collectors, they first require the uniform coating with conductive electrode materials. A variety of conductive materials, including carbon nanotubes (CNTs), reduced graphene oxides (rGOs), and metal nanowires (NWs), have been incorporated into cellulose fibril-based papers or textiles through conventional physical adsorption processes (e.g., via a doctor blade, simple physical soaking, spraying, and the Meyer rod coating process).<sup>[23–26]</sup> However, these conductive papers or textiles exhibit relatively low electrical conductivity (sheet resistance  $> 10 \Omega \text{ sq}^{-1}$  and electrical conductivity  $< 300 \text{ S cm}^{-1}$ ) due to the significant contact resistance among adjacent conductive materials. Moreover, conventional physical coating processes have difficulty preserving the porous structure of pristine papers or textiles due to the agglomeration and nonuniform coating of conductive components. Chemical reduction of metal precursor ions from solution (i.e., the electroless [EL] metal deposition method) has also been used to prepare conductive paper or textile current collectors. However, in most cases, chemically reduced metals have a lower conductivity than bulk metals due to the presence of organic impurities in the metal precursors. Additionally, this approach can cause a considerable decrease in conductivity under various mechanical stimuli, such as bending or crumpling, because of the unfavorable interfacial adhesion between the substrate and

the chemically reduced metal layer. It is particularly difficult to control the structure and uniformity of the chemically reduced metal coating on the substrate, which can lead to agglomeration and a nonuniform coating that can block pores, decreasing accessible surface area. Therefore, EL deposition has some limitations in preparing paper- or textile-based electrodes that require high areal performances. It should be noted that the areal loading of the active material and the effectiveness of charge transfer between the current collector and the active material, play pivotal roles in determining the performance of flexible electrodes. Thus, there is an urgent need to develop new processes for the deposition of conductive materials on 3D flexible substrates that enable high conductivity, high areal performance, and excellent mechanical properties

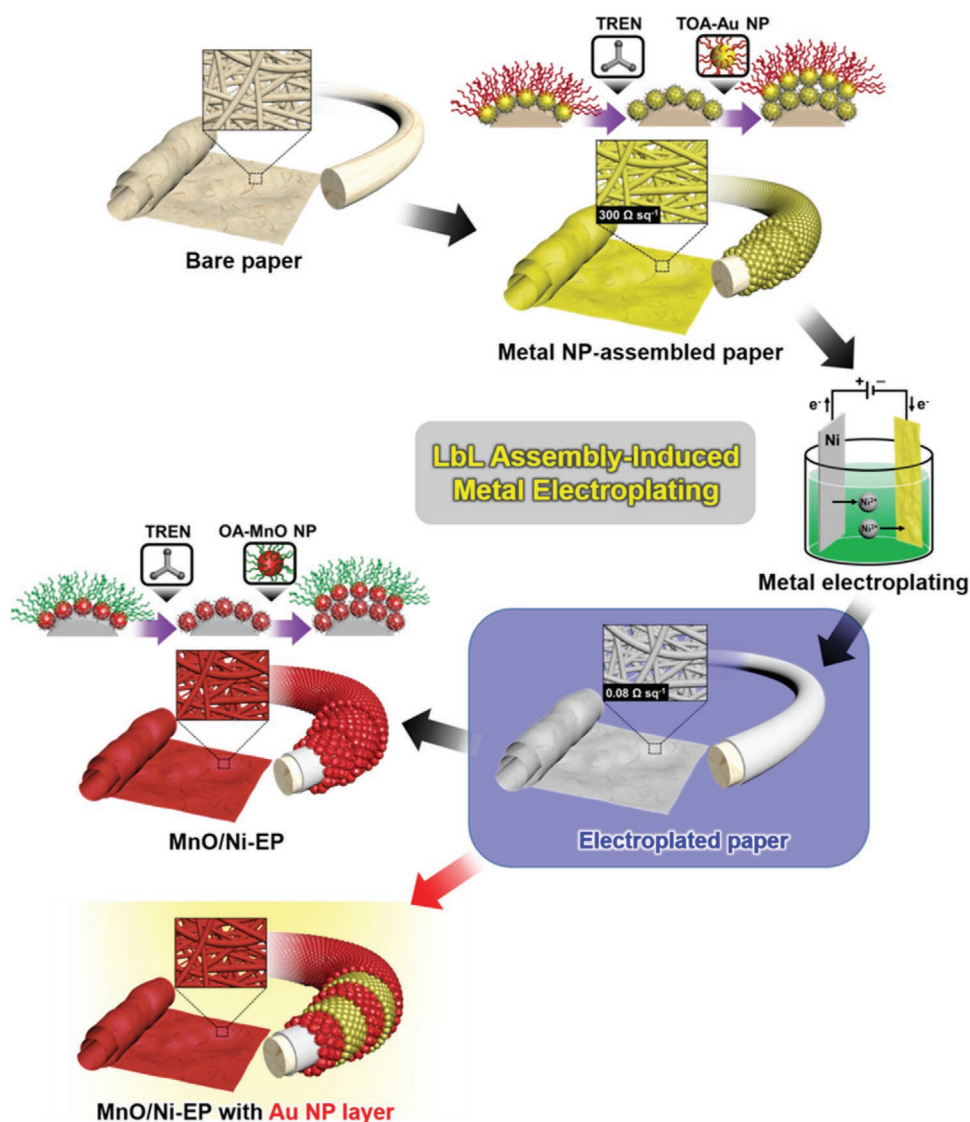
Metal electrodeposition approach has been also applied to the textile substrates for preparing 3D-current collectors.<sup>[27,28,30,31]</sup> This approach has been considered as an effective method in the sense that it allows the deposition of metal layers onto the substrates without any impurities originated from precursors or reducing agents. However, as mentioned earlier, to prepare the metal-electrodeposited papers or textiles, they should first possess the electrical conductivity suitable for electrodeposition. For this goal, the chemical reduction of metal precursor ions (i.e., electroless deposition) has been introduced into the insulating textiles, and then metal electroplating has been carried out on the conductive textiles. However, this approach presents much difficulty in forming a uniform metal layer onto the conductive textiles because the electrodeposited metal layer is selectively formed onto chemically reduced metal clusters with aggregated and/or nonuniform coating. Instead of this electroless deposition, a carbonization process has been also utilized as a pretreatment for endowing electrical conductivity to the insulating textiles.<sup>[30,31]</sup> However, this carbonization approach requires high heating temperature (>900 °C) to form a network of sp<sup>2</sup> hybridized carbon-carbon bonds and generate mobile pi ( $\pi$ )-electrons. Moreover, thermal decomposition during the carbonization process induces a serious thermal shrinkage of pristine textiles, and furthermore can have a detrimental effect on their mechanical flexibility. As such, the carbonization process for metal electrodeposition is inadequate for paper- or textile-based current collectors that require the large surface area and mechanical flexibility of pristine textiles or papers.<sup>[32,33]</sup> Therefore, the desirable metal deposition should provide sufficient electrical conductivity to the insulating papers or textiles without physical and/or chemical damages.

A layer-by-layer (LbL) assembly method is based on complementary, mainly electrostatic interactions between neighboring components. This process enables the fabrication of conformal multilayer thin films with various functionalities and thicknesses tunable at the nanometer level onto various substrates irrespective of their size and shape.<sup>[34–47]</sup> However, using the traditional electrostatic LbL assembly method, metal nanoparticle (NP)-based multilayer films suffer from high contact resistances. This is a result of the large separation distances due to the low packing density of metal NPs and insulating polymer linkers and/or organic ligands bound to the surface of metal NPs, and thus have significantly decreased electrical conductivity.<sup>[39,46]</sup> To enhance their conductivity,

these films need additional thermal treatment and/or mechanical pressing,<sup>[46]</sup> which may have a detrimental effect on the porous structure of heat- and/or pressure-sensitive textile substrates. Recently, we have reported a small-molecule linker-mediated LbL assembly method that can overcome these challenges for assembling 3D conductive electrodes.<sup>[13]</sup> Although this approach allows the assembly of various NPs on 3D paper and textile substrates with controlled interparticle distances and interfacial structure, at least dozens of Au NP layers needed to be deposited onto the papers to obtain a high conductivity. Specifically, 10 and 30 Au NP layers onto papers resulted in  $\approx 2$  and  $0.2 \Omega \text{ sq}^{-1}$ , respectively. This repetitive LbL process also required a relatively long deposition time.

Herein, we introduce a novel approach (i.e., LbL assembly-induced electroplating approach) to prepare paper or textile electrodes with bulk metal-like conductivity, paper-like flexibility, and a highly porous structure (**Scheme 1**). We highlight that our approach can resolve the drawbacks of previously reported approaches by combining a small-molecule linker-mediated LbL assembly and metal electrodeposition. An LbL assembly-induced electroplating approach shows that various metals (Ni, Cu, Ag, etc.) can be uniformly electroplated onto the various flexible substrates with only a few layers of LbL-assembled Au, Ag, or Cu NPs, and their electrical conductivities outperform those of conductive papers or textiles reported to date. Furthermore, we demonstrate that the electroplated metal papers can be effectively used as current collectors for high-performance energy storage electrodes. For this study, metal NPs (i.e., tetraoctylammonium [TOA]-stabilized Au NPs) were first LbL-assembled with small organic linkers (tris(2-aminoethyl) amine [TREN]) onto papers. In this case, TOA-Au NPs can be replaced by other metal NPs such as TOA-Ag NPs and TOA-Cu NPs (this evidence is given in the latter part). After deposition of only a few bilayers onto the bare papers, a subsequent Ni electroplating process produced a highly flexible Ni paper with an extremely low sheet resistance value of  $\approx 0.08 \Omega \text{ sq}^{-1}$ . We highlight that the abovementioned Ni-electroplated papers (Ni-EPs) can be prepared after deposition of only four bilayers of metal NPs. This improvement is in stark contrast to the previously reported metallic paper<sup>[13]</sup> or highly conductive elastomer<sup>[47]</sup> that required many more metal NP layers. We also show that our approach can be directly extended to produce the electroplated papers using a variety of other metals, such as Au, Ag, and Cu, in addition to Ni.

Another interesting phenomenon is that metal electroplating onto papers or textiles composed of numerous fibrils allows the creation of a uniform metal coating onto the respective fibrils, maintaining their intrinsic internal structure without blocking pores. This unique approach (i.e., LbL assembly-induced metal electroplating) can also be effectively applied to flexible supercapacitor electrodes with high areal capacitance values. The subsequent deposition of MnO NPs stabilized with oleic acid ligands (OA-MnO NPs) and small-molecule linkers onto the Ni papers generates a high areal capacitance of  $811 \text{ mF cm}^{-2}$  at a MnO NP mass loading of  $4.31 \text{ mg cm}^{-2}$ . This capacitance can be further increased by increasing the mass loading of OA-MnO NPs and by intercalating a conductive metal NP layer between adjacent MnO NP layers with poor conductivity, yielding an



**Scheme 1.** Schematic illustration of the metal-like conductive paper electrodes based on LbL Au nanoparticle assembly followed by Ni electroplating.

areal capacitance of up to  $1710 \text{ mF cm}^{-2}$  due to the improved charge transfer. Our approach can be effectively applied to various insulating papers or textiles, and the charge transfer within electrodes can be significantly enhanced by the controlled interfacial interactions and the insertion of metal NPs. We therefore believe that a metal NP assembly-induced electroplating approach can provide an important tool for developing high-performance 3D electrodes for various energy storage and conversion devices.

## 2. Results and Discussion

### 2.1. Preparation of Metallic Textile Using LbL-Assembly-Induced Metal Electroplating

In developing a 3D current collector for supercapacitor electrodes, we primarily investigated the development of highly

porous conductive paper based on Korean traditional paper “Hanji” due to its high mechanical flexibility and large surface area. We first sought to characterize the adsorption behavior of the  $(\text{TOA-Au NP/TREN})_n$  multilayers using UV-vis spectroscopy and a quartz crystal microbalance (QCM).  $5 \text{ mg mL}^{-1}$  suspension of TOA-stabilized Au NPs, with a diameter of  $\approx 8 \text{ nm}$ , in toluene and a  $1 \text{ mg mL}^{-1}$  solution of amine  $(\text{NH}_2)$ -functionalized TREN in ethanol were employed to form the multilayers through LbL assembly (Figure S1, Supporting Information). For this study, the adsorption times of TOA-Au NPs and TREN were 30 and 10 min, respectively. As the bilayer number ( $n$ ) of  $(\text{TOA-Au NP/TREN})_n$  was increased to 10, the surface plasmon resonance absorption peak of TOA-Au NP layers measured from UV-vis spectroscopy shifted substantially to higher wavelengths in the near-infrared (IR) region (Figure S1c, Supporting Information). This phenomenon indicates that the packing density of adsorbed TOA-Au NPs gradually increased in both the lateral and vertical dimensions (i.e., a reduced interparticle distance

between Au NPs). The alternating deposition of TOA-Au NPs and TREN resulted in a frequency change ( $-\Delta F$ ) of  $382.6 \pm 50$  Hz (or mass change ( $\Delta m$ )  $\approx 6.76 \pm 0.8 \mu\text{g cm}^{-2}$ ) per bilayer number. The decrease in  $\Delta m$  during the deposition of TREN suggests that bulky TOA ligands loosely bound to the surface of the Au NPs were replaced by relatively small TREN molecules due to the comparatively high affinity between the Au NP surfaces and the  $\text{NH}_2$  moieties of TREN during this LbL deposition. This ligand exchange reaction in the LbL-assembled films was also confirmed by Fourier transform infrared (FT-IR) spectroscopy (Figure S2, Supporting Information). In line with these results, the thickness of the  $(\text{TOA-Au NP/TREN})_n$  multilayers increased almost linearly with the increase in the bilayer number ( $n$ ) (Figure S3, Supporting Information).

With this knowledge of bilayer absorption and thickness,  $(\text{TOA-Au NP/TREN})_n$  multilayers were deposited onto 100  $\mu\text{m}$ -thick paper substrates composed of hydroxyl (OH) group-functionalized cellulose fibers. To this end, the TREN layer was first deposited onto the paper for the preparation of  $\text{NH}_2$ -functionalized paper, and then TOA-Au NPs can be uniformly coated onto the TREN-coated paper through the consecutive ligand exchange reactions between bulky TOA ligands and small TREN linkers. However, after only one or two bilayer deposition cycles, the paper still exhibited insulating properties because of the numerous contact resistance points occurring among the spherical-type Au NPs as well as insufficient surface coverage of Au NPs. The paper with three bilayers also exhibited a high sheet resistance of  $8.43 \times 10^5 \Omega \text{ sq}^{-1}$  and a low electrical conductivity of  $1.5 \times 10^{-3} \text{ S cm}^{-1}$ . However, with increasing  $n$  from 4 to 10, the sheet resistance and electrical conductivity of paper dramatically changed from  $300 \Omega \text{ sq}^{-1}$  and  $0.56 \text{ S cm}^{-1}$  to  $2.77 \Omega \text{ sq}^{-1}$  and  $38 \text{ S cm}^{-1}$  (including a paper thickness of 100  $\mu\text{m}$ ), respectively (Figure 1a). Particularly, we noted that the four bilayer-coated paper with densely packed Au NPs had sufficiently low sheet resistance applicable to commercial electroplating (Figure S4, Supporting Information). It is interesting to envision the possibility that metal-like conductive papers can be easily and quickly prepared through metal electroplating with the aid of a minimal number of metal NP layers, and furthermore the electroplated metal layer can be uniformly coated onto all the respective cellulose fibrils within paper. Although the sheet resistance of the paper with three bilayers is likely too high, the four bilayer-coated paper (i.e.,  $(\text{TOA-Au NP/TREN})_4$ -coated paper) with the sheet resistance of  $300 \Omega \text{ sq}^{-1}$  can have the potential for this objective without further LbL NP deposition. Additionally, we confirmed that the mechanical and electrical properties of  $(\text{TOA-Au NP/TREN})_4$ -coated paper were very stable under repeated external stimuli (Figure S5, Supporting Information).

To confirm this possibility, Ni-electroplating using two-electrode-configuration system was carried out onto the  $(\text{TOA-Au NP/TREN})_4$ -coated paper (Figure S6, Supporting Information). First, we examined the change in the sheet resistance of  $(\text{TOA-Au NP/TREN})_4$  multilayer-coated paper as a function of both external current density and electroplating time in an aqueous electrolyte solution containing nickel precursors. As shown in Figure 1b, when the current density and electroplating time were increased from  $25 \text{ mA cm}^{-2}$  and 2 min to  $250 \text{ mA cm}^{-2}$  and 10 min, respectively, the sheet resistance of

Ni-EPs (sample size  $\approx 1 \text{ cm} \times 4 \text{ cm}$ ) was decreased to  $0.08 \Omega \text{ sq}^{-1}$  (the sheet resistance of commercial bulk Ni is  $\approx 10^{-4} \Omega \text{ sq}^{-1}$ ), outperforming the previously reported paper- or textile-type electrodes in terms of electrical properties.<sup>[13,45,48]</sup> Furthermore, we quantitatively investigated the effect of LbL-assembled films on the physical and electrical properties of the Ni electroplating products. For this investigation, the Ni electroplating process was performed on  $(\text{TOA-Au NP/TREN})_n$ -coated papers ( $n = 4-10$ ) using a fixed external current density of  $250 \text{ mA cm}^{-2}$  and an electroplating time of 10 min. As the number of TOA-Au NP/TREN bilayers increased from 4 to 10, the thickness of the electroplated Ni layer increased from  $\approx 0.45$  to  $1.19 \mu\text{m}$  (Figure 1c). According to the increase in the thickness of electroplated Ni layer, the sheet resistance of the electroplated Ni- $(\text{TOA-Au NP/TREN})_n$  papers was slightly decreased from  $\approx 0.08$  (for  $n = 4$ ) to  $0.06 \Omega \text{ sq}^{-1}$  ( $n = 10$ ), and additionally the corresponding electrical conductivity was increased from 830 to  $1013 \text{ S cm}^{-1}$  (factoring in a paper thickness of 100  $\mu\text{m}$ ) (Figure 1d). That is, these results imply that if the  $(\text{TOA-Au NP/TREN})_n$  paper possesses sufficient electrical conductivity for electroplating, a further increase in the bilayer number does not have a critical effect on the electrical conductivity of Ni-EPs.

We also investigated the thickness of electroplated Ni layer onto the  $(\text{TOA-Au NP/TREN})_4$ -coated paper as a function of electroplating time at fixed current density of  $250 \text{ mA cm}^{-2}$ . In this case, the thickness of Ni layer was increased from 0.14 (for 2 min) to  $1.17 \mu\text{m}$  (for 20 min) (Figure 1e). Additionally, it should be noted that our approach can also be applied to other textiles such as cotton (Figure S7, Supporting Information), and furthermore the thickness of electroplated metal layer onto papers or textiles could be controlled by bilayer number of LbL-assembled metal NP layers, electroplating time, and electroplating current density.

For understanding the conductivity mechanism of conductive papers, temperature-dependent electrical resistivity tests for the  $(\text{TOA-Au NP/TREN})_4$  paper and the electroplated Ni- $(\text{TOA-Au NP/TREN})_4$  paper were carried out using a physical property measurement system over a temperature range from 2 to 300 K (Figure 1f and Figure S8, Supporting Information). In this case, the electrical resistivity of the  $(\text{TOA-Au NP/TREN})_4$  paper gradually decreased as the temperature decreased, showing typical metallic behavior (Figure 1f). Therefore, this conductive paper displayed a positive temperature coefficient ( $\alpha$ ) that is characteristic of a metal, as shown in Equation (1). This relation is defined as follows:<sup>[13,37]</sup>

$$\Delta R/R_0 = \alpha \Delta T \quad (1)$$

where  $R$  is the resistance ( $\Omega$ ),  $\alpha$  is the temperature coefficient ( $\text{K}^{-1}$ ), and  $T$  is the absolute temperature (K).

When Ni was electroplated onto the  $(\text{TOA-Au NP/TREN})_4$  papers for 2 and 10 min, the metallic conductivities of the Ni-EPs increased with increasing electroplating time and showed an increase in the temperature coefficient. That is, the higher the positive temperature coefficient, the higher an increase in electrical resistance for a given temperature increase. We also confirmed that these conductivity behaviors of Ni-EPs and LbL-assembled Au NP-coated papers are not fitted by the hopping conduction mechanism model that can be expressed with the following relation:<sup>[49]</sup> (Figure S8, Supporting Information)

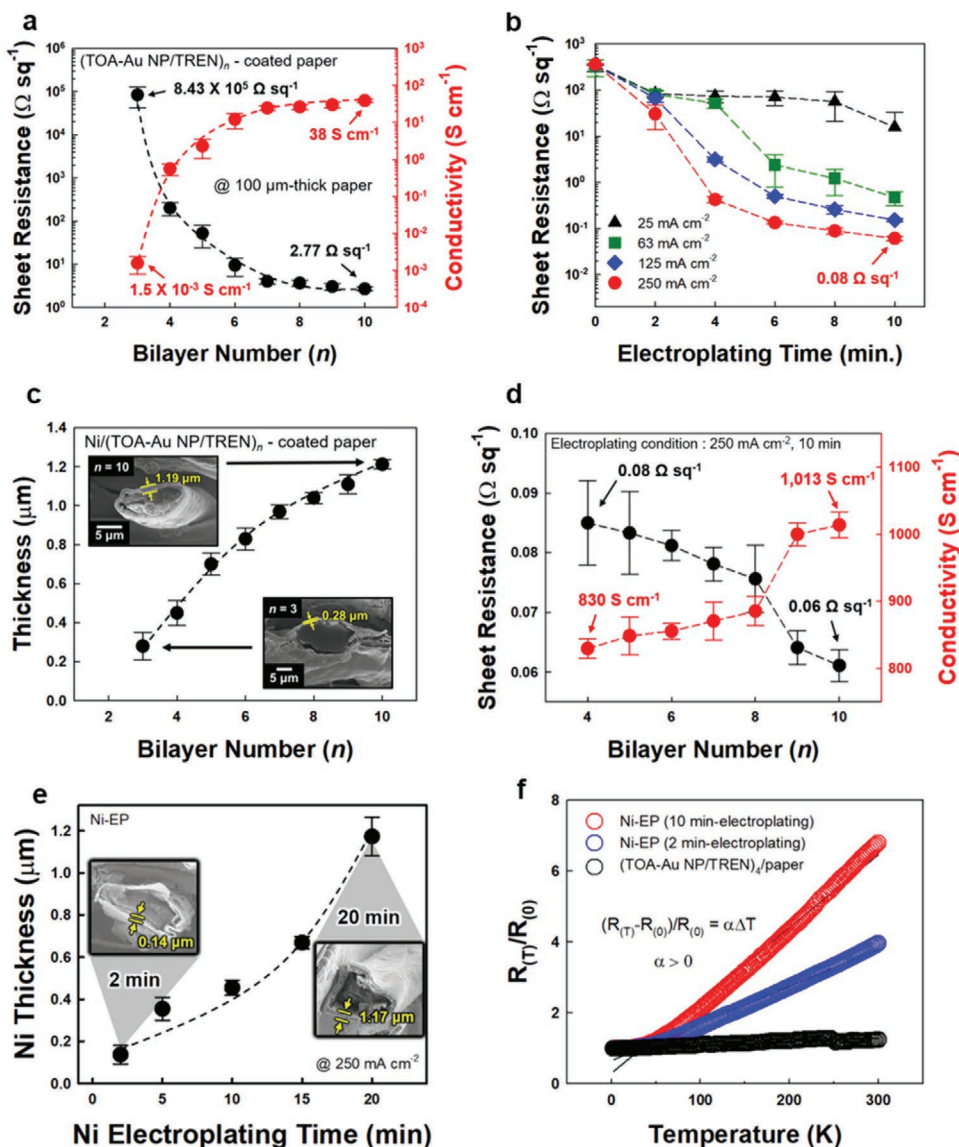


**Figure 1.** Physical properties of the Ni-electroplated paper (Ni-EP) electrodes. a) Electrical properties of the (TOA-Au NP/TREN)<sub>n</sub>-coated paper electrodes with increasing bilayer number ( $n$ ). b) Sheet resistance values of Ni-electroplated (TOA-Au NP/TREN)<sub>4</sub> paper electrodes as a function of external current density and electroplating time. c) Thickness data and FE-SEM images (insets) of the electroplated Ni layer on the fiber of paper electrodes with increasing bilayer number of the (TOA-Au NP/TREN)<sub>n</sub> multilayer (fixed external current density and electroplating time of 250  $\text{mA cm}^{-2}$  and 10 min, respectively.) d) Electrical properties of Ni-EP electrodes with increasing bilayer number of the (TOA-Au NP/TREN)<sub>n</sub> multilayer. e) Thickness of electroplated Ni layer onto (TOA-Au NP/TREN)<sub>4</sub>-coated paper as a function of electroplating time at the fixed current density of 250  $\text{mA cm}^{-2}$ . f) Plots of the resistance ( $R_{(T)}/R_{(0)}$ ) versus temperature (K) for (TOA-Au NP/TREN)<sub>4</sub> paper and Ni-EPs (electroplating time = 2 and 10 min).

$$\sigma = \sigma_0 \exp\left(-A/T^{1/(d+1)}\right) \quad (2)$$

where  $\sigma$  and  $\sigma_0$  are the conductivities,  $A$  is a constant,  $T$  is the absolute temperature, and  $d$  is the dimensionality ( $d = 3$  in the hopping mechanism).

In addition to the high conductivity, another feature exhibited by the Ni-EP is that electroplated Ni is uniformly and homogeneously deposited onto the cellulose fibrils within the paper. As confirmed by field-emission scanning electron microscopy (FE-SEM) and energy dispersive X-ray spectroscopy (EDS), the Ni-EP (i.e., Ni/(TOA-Au NP/TREN)<sub>4</sub> paper prepared from Ni electroplating condition of 250  $\text{mA cm}^{-2}$  for

10 min) maintained its porosity without blocking of porous fabric structure by Ni agglomeration (Figure 2a–c). Additionally, the electroplated Ni layer exhibited highly protuberant but dense surface morphology consisting of nano-scale Ni clusters. (Figure 2a and Figure S9, Supporting Information). Therefore, the pore area per unit mass ( $\approx 1.140 \text{ m}^2 \text{ g}^{-1}$ ) of Ni-EP was larger than that ( $\approx 0.789 \text{ m}^2 \text{ g}^{-1}$ ) of bare paper despite the high mass of electroplated Ni as confirmed by mercury porosimetry technique (Figure S10, Supporting Information). These results evidently imply that an increased surface area of Ni-EP originates from protuberant structure of electroplated Ni/(TOA-Au NP/TREN)<sub>4</sub> multilayers.

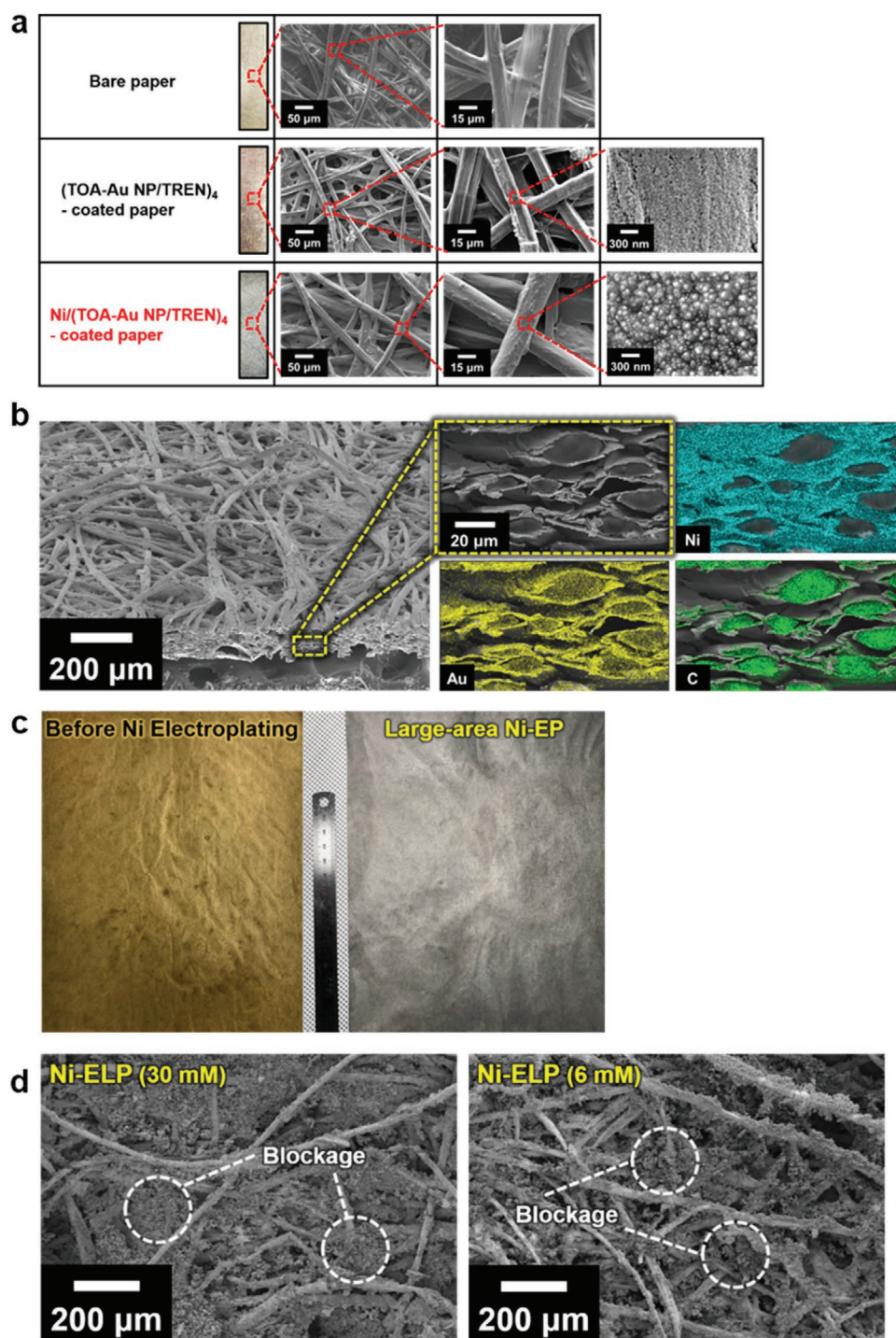


**Figure 2.** Photographic, FE-SEM, and EDS mapping images of the paper electrodes. a) Photographic (left) and FE-SEM images at different magnifications (right) of bare paper, (TOA-Au NP/TREN)<sub>4</sub>-coated paper and Ni/(TOA-Au NP/TREN)<sub>4</sub>-coated paper. b) Tilted FE-SEM and EDS mapping images of the cross-section of Ni/(TOA-Au NP/TREN)<sub>4</sub>-coated paper. c) Photographic image of large-area (20 cm × 30 cm) (TOA-Au NP/TREN)<sub>4</sub>-coated paper and Ni-EP. d) FE-SEM images of Ni-coated paper prepared with electroless plating in solutions of different concentrations (30 and 6 mM of NiSO<sub>4</sub>·6H<sub>2</sub>O in deionized water).

Particularly, the EDS images of Figure 2b evidently show that Ni atoms and Au atoms were uniformly observed in all the areas on the surface of the cellulose fibrils ranging from the exterior to the interior of the paper substrate. Given

that this combined approach, using both ligand exchange LbL assembly and the metal electroplating process, is not seriously restricted by the substrate size or shape, it is worth noting that large-area metal-like conductive papers or

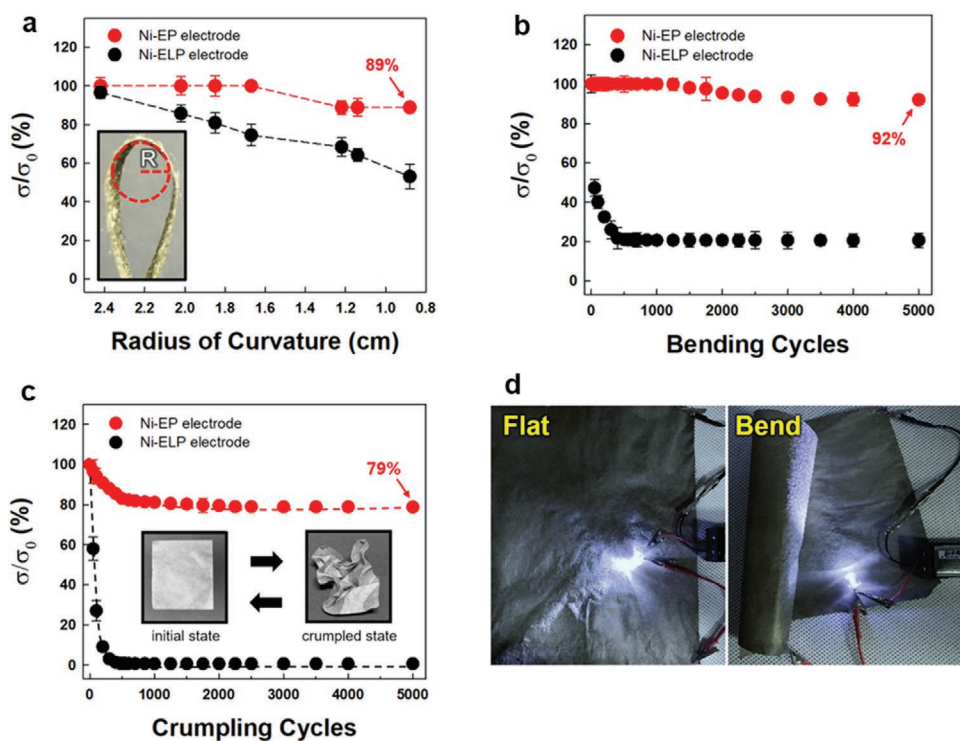


**Figure 3.** a) Relative electrical conductivity ( $\sigma/\sigma_0$ ) of Ni-EP and Ni-ELP electrodes as a function of the radius of curvature ( $R$ ). b) Relative electrical conductivity of Ni-EP and Ni-ELP electrodes as a function of bending cycling number (bending radius of  $\approx 1.7$  cm). c) Relative electrical conductivity of Ni-EP and Ni-ELP electrodes as a function of crumpling cycling number. d) Photographic images of Ni-EP with an LED connection in flat and bent states.

textiles can be easily prepared by our approach, as shown in Figure 2c.

On the other hand, the electroless deposition approach has many difficulties in preparing large-area conductive papers or textiles with a highly uniform coating of the Ni layer due to the complex process variables, including the metal precursor concentration, the reducing agent concentration, and/or the reaction time. As shown in Figure 2d, Ni-electroless deposited paper (Ni-ELP), prepared from same type of paper, exhibited Ni agglomeration on the outermost surface of the paper without achieving a uniform distribution of Ni on the interior of the paper. This nonuniform deposition resulted in a higher sheet resistance,  $\approx 1.4 \Omega \text{ sq}^{-1}$ , than that of Ni-EP due to organic impurities existing within electroless deposited Ni layers (see the Experimental Section).

An additional benefit of Ni-electroplated paper (Ni-EP) electrodes is their ability to maintain high electrical conductivity under external mechanical stress such as bending. To demonstrate this capability, the conductivity change ( $\sigma/\sigma_0$ ) in Ni/(TOA-Au NP/TREN)<sub>4</sub> paper, with the conductivity of  $830 \text{ S cm}^{-1}$  (sheet resistance of  $0.08 \Omega \text{ sq}^{-1}$ ) at the initial (flat) state (conductivity at initial state  $\approx \sigma_0$ ), was investigated as a function of the bending radius, bending cycles, and crumpling cycles (Figure 3). First, as the radius of the bending curvature decreased from 2.4 to 0.9 cm, the electrical conductivities of Ni-EP and Ni-ELP decreased to 89 and 54% of the initial conductivities, respectively (Figure 3a). Bending cycling tests were performed on Ni-EP and Ni-ELP with radius of curvature of

$\approx 1.7$  cm. Even after 5000 cycles, the electrical conductivity of Ni-EP remained at 92% of the initial conductivity, which was in stark contrast to that of the Ni-ELP, which retained only  $\approx 20\%$  of its initial conductivity, as shown in Figure 3b. Similarly, the combined durability of the conductivity and mechanical flexibility of Ni-EP was also confirmed by crumpling cycling tests (Figure 3c). However, in the case of Ni-ELP, its relative electrical conductivity was reduced to almost 0% after 30 cycles. On the other hand, the Ni-EP exhibited 79% of its initial conductivity even after 5000 cycles of the harsh crumpling test. Figure 3d displays images of highly conductive Ni-EPs with a functioning LED connection in flat and bent states, visually showing that their conductivity is maintained in various physical conformations. These results demonstrate that our approach is effective in preparing conductive papers with electrical stability under various mechanical stimuli.

We also investigated the possibility that the metal NP assembly-induced electroplating approach could also be applied to various textile-type substrates with porous structure, such as cotton, nylon, and polyester, which have a high affinity (hydrogen-bonding interaction) with the amine groups of TREN. As shown in Figure 4a, the Ni electroplating (i.e., external current density and electroplating time of  $250 \text{ mA cm}^{-2}$  and 10 min, respectively) after the deposition of (TOA-Au NP/TREN)<sub>4</sub> multilayers onto the textiles caused the surfaces of all the respective fibrils to be uniformly coated with Ni, resulting in extremely low sheet resistances (i.e.,  $0.4 \Omega \text{ sq}^{-1}$  for cotton,  $0.8 \Omega \text{ cm}^{-1}$  for nylon, and  $0.08 \Omega \text{ sq}^{-1}$

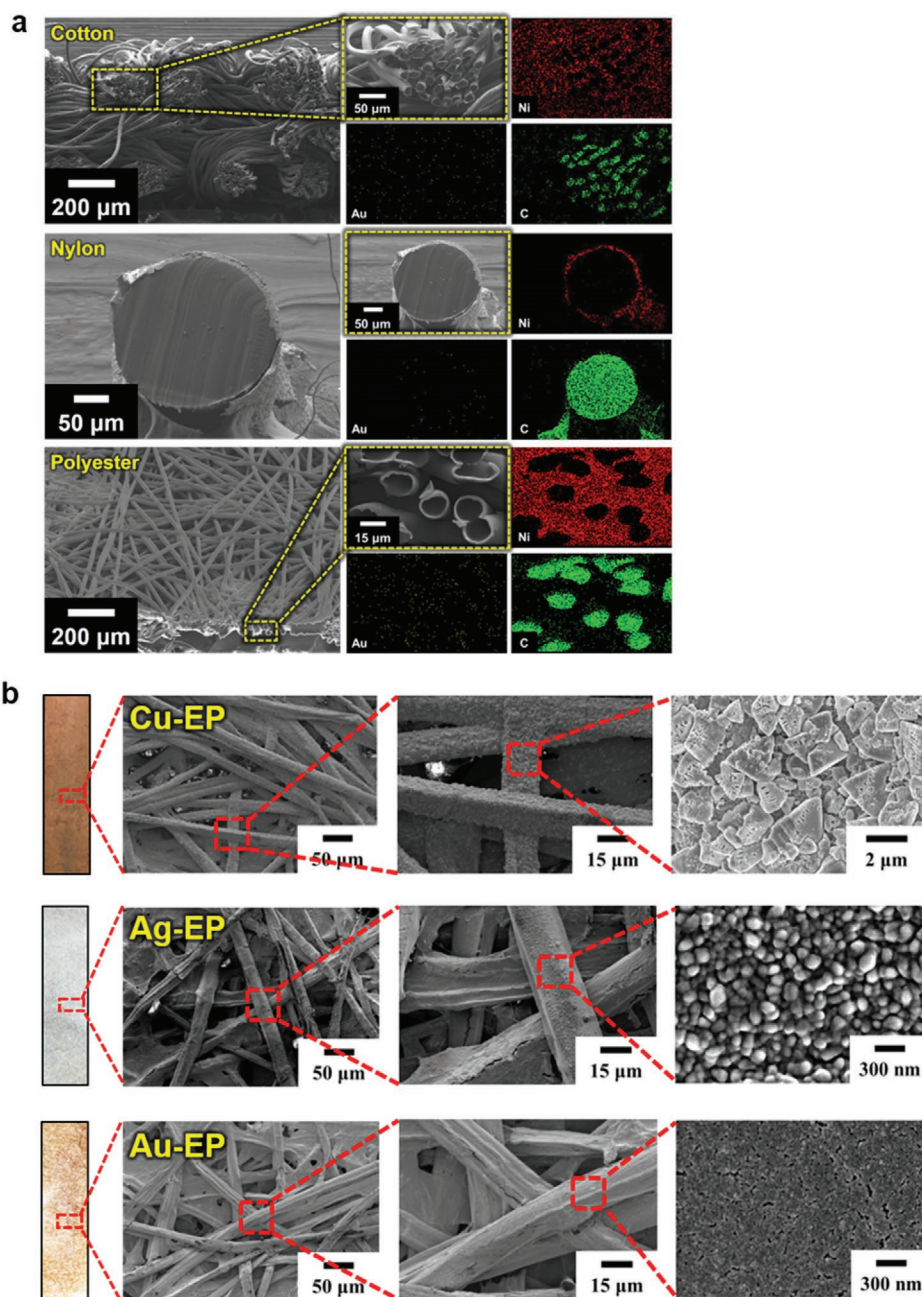


**Figure 4.** a) Tilted and cross-sectional FE-SEM and EDS mapping images of Ni-electroplated textiles: cotton (top), nylon (middle), and polyester (bottom). b) Photographic and FE-SEM images of paper electrodes electroplated with Cu (top), Ag (middle), and Au (bottom). The Cu-, Ag-, and Au-EPs were prepared by electroplating with current density of  $250 \text{ mA cm}^{-2}$ .

for polyester). Additionally, the difference between the sheet resistance values of Ni-electroplated cotton, nylon, and polyester textiles can be caused by the loading amount of TOA-Au NPs adsorbed onto the textiles. That is, the higher loading of TOA-Au NPs onto textile induces the higher electrical conductivity, which can increase the thickness of electroplated-Ni layer at the same electroplating condition. Furthermore, our approach can be effectively used for the preparation of Cu- and Ag-EPs as well as Au-EPs with same electroplating conditions

( $250 \text{ mA cm}^{-2}$ , 10 min), as shown in Figure 4b. Furthermore, it should be noted that the TOA-Au NPs used for conductive paper or textiles before electroplating can be replaced by other metal NPs such as TOA-Cu NPs and TOA-Ag NPs (Figures S11 and S12, Supporting Information). These results show that a variety of flexible and metallic papers or textiles with porous structures can be easily prepared, with the possibility of being utilized as electrochemical electrodes in numerous applications requiring a large specific surface area and high conductivity.

## 2.2. Electrochemical Performance of MnO NP-Incorporated Metallic Textile

To demonstrate the potential relevance of our approach in energy applications, we explored the possibility of using Ni-EPs (i.e., Ni/(TOA-Au NP/TREN)<sub>4</sub> paper) as 3D current collectors and supercapacitor energy reservoirs. To achieve this goal, (TOA-Au NP/TREN)<sub>n</sub> ( $n = 4$ ) multilayers were assembled onto a paper substrate, and Ni was electroplated onto the (TOA-Au NP/TREN)<sub>4</sub> multilayer-coated papers at a current density of 250 mA cm<sup>-2</sup> for 10 min. After Ni electroplating was performed, pseudocapacitive oleic acid (OA)-stabilized MnO NPs (OA-MnO NPs) with a diameter of ≈7 nm were sequentially LbL assembled with TREN molecules onto the Ni-EPs (Figure 5a). As with the TOA-Au NP/TREN multilayer system, this LbL assembly was based on the consecutive ligand exchange reactions, which was induced by the higher affinity of the MnO NP surfaces for the NH<sub>2</sub> groups of TREN molecules than for the carboxylate ions of the original OA ligands (Figure S13, Supporting Information). Therefore, bulky OA ligands were replaced by TREN molecule linkers during LbL deposition, and resultantly the organics existing between adjacent MnO NPs are only TREN molecule layers. It should also be noted that TREN molecules have a high affinity with various metal and metal oxides including Ni, NiO, and MnO. Therefore, TREN molecules could directly connect all the interfaces between both vertically neighboring MnO NPs, between the Ni paper and MnO NPs, between neighboring Au NPs as well as between paper and Au NPs. These phenomena were also confirmed by the fact that water droplet was completely infiltrated into the outermost TREN-coated electrode (i.e., 20-MnO NP/Ni-EP electrode) (Figure S14, Supporting Information).

OA-MnO NPs were uniformly deposited onto all the regions ranging from the exterior to the interior of the Ni-EPs (Figure S15, Supporting Information). The mass loading of (OA-MnO NP/TREN)<sub>m</sub> (i.e., *m*-MnO NP) multilayers on the porous Ni-EP increased linearly with the bilayer number (*m*) of *m*-MnO NP, which was ≈19 times higher than the adsorbed mass loading on nonporous electrodes (i.e., flat QCM electrodes) at the same bilayer number (i.e.,  $m = 140$ ) (Figure 5b). Specifically, the average mass loadings of 1 bilayer (i.e., (OA-MnO NP/TREN)<sub>1</sub>) onto Ni-EP and nonporous electrodes were measured to be ≈30.78 and 1.64 μg cm<sup>-2</sup>, respectively. Considering that the mass ratio of pure MnO NPs to OA-MnO NP/TREN multilayers is ≈87.6% as confirmed by thermogravimetric analysis (TGA) (Figure S16, Supporting Information), the loading amount of MnO NPs per bilayer onto the Ni-EP and nonporous electrodes were calculated to be ≈29.9 and 1.60 μg cm<sup>-2</sup>, respectively. These results indicate that the loading amount of pseudocapacitive MnO NPs can be enhanced both by employing the high surface area Ni-EP and by increasing the number of MnO/TREN bilayers.

Based on these results, we investigated the possibility that *m*-MnO NP-coated Ni-EPs (i.e., *m*-MnO NP/Ni-EP) can be effectively used as supercapacitor electrodes. First, for this goal, the cyclic voltammetry (CV) scans of the 20-MnO NP multilayers assembled onto the Ni-EP and nonporous Ni electrodes were conducted at scan rates of 50 mV s<sup>-1</sup> in a three-electrode cell configuration with 0.5 M Na<sub>2</sub>SO<sub>4</sub> (Figure 5c). The 20-MnO

NP/Ni-EP electrode delivered a significantly enhanced current density compared to those of the bare Ni-EP and 20-MnO NP/nonporous electrodes. A notable increase in the integrated CV area as well as the current density of 20-MnO NP/Ni-EP electrode can be attributed to the effective utilization of the high pseudocapacitance of MnO NPs<sup>[50]</sup> through the 3D Ni-EP. Additionally, the 20-MnO NP/Ni-EP electrode with MnO NP mass loading of 0.62 mg cm<sup>-2</sup> exhibited good rate performance at scan rates up to 500 mV s<sup>-1</sup> due to the relatively facile charge transfer characteristics (Figure 5d and Figure S17, Supporting Information). Specifically, the areal capacitances of the 20-MnO NP/Ni-EP electrode were 199 mF cm<sup>-2</sup> at a slow scan rate of 5 mV s<sup>-1</sup> and 86 mF cm<sup>-2</sup> at a faster scan rate of 200 mV s<sup>-1</sup> (Figure 5d).

We also investigated the bilayer number (*m*)-dependent CV scans and the specific capacitances of *m*-MnO NP/Ni-EP electrodes as a function of the OA-MnO NP/TREN bilayer number (*m*) (Figure 5e,f). Although the current densities of the CV scans at 5 mV s<sup>-1</sup> gradually increased with the bilayer number, the specific capacitance of the *m*-MnO NP/Ni-EP electrodes rapidly decreased from 458 to 188 F g<sup>-1</sup> as *m* increased from 5 (with a mass loading of MnO NPs of 0.15 mg cm<sup>-2</sup>) to 140 (4.31 mg cm<sup>-2</sup>). This dramatic decrease in the specific capacitance was mainly due to an increase in electrical resistance through MnO NP arrays with poor electrical conductivity, which was confirmed by electrochemical impedance spectroscopy (EIS) (Figure 5g). In this case, the equivalent series resistance (*R*<sub>s</sub>) and charge transfer resistance (*R*<sub>ct</sub>) values of the *m*-MnO NP/Ni-EP electrodes increased from 2.9 and 0.016 to 10.9 and 3.1 Ω cm<sup>2</sup>, respectively, with an increase in *m* from 5 to 140. We also investigated the electrochemical stability of *m*-MnO NP/Ni-EP at a high current density that can be much more meaningful for practical use. To this end, galvanostatic charge/discharge (GCD) curves of 60-MnO NP/Ni-EP electrode were first obtained in current density range from 2 (1.1 A g<sup>-1</sup>) to 20 mA cm<sup>-2</sup> (10.8 A g<sup>-1</sup>), which displayed the typical characteristic of pseudocapacitive behavior (Figure S19, Supporting Information). In addition, we confirmed that the 60-MnO NP/Ni-EP electrode exhibited good cycling stability by maintaining 71.3% of its initial capacitance even after 1000 cycles at current density of 10 mA cm<sup>-2</sup> (5.4 A g<sup>-1</sup>) (Figure S20, Supporting Information).

Accordingly, the 140-MnO NP/Ni-EP electrode could deliver a high areal capacitance of 811 mF cm<sup>-2</sup> at 5 mV s<sup>-1</sup>, but its capacitance quickly decreased with increasing scan rate (Figure 5h). Although it was reported that the electrodeposited MnO<sub>2</sub> onto the current collector could exhibit good rate performance,<sup>[51]</sup> such performance could be observed from electrodeposited MnO<sub>2</sub> with a relatively low loading mass. Therefore, in the case of electrodepositing high mass loading of MnO<sub>2</sub> onto our Ni-EP current collector, their areal capacity was also dramatically decreased with increasing the scan rate (Figure S21, Supporting Information).

Additionally, we exclude the possibility that a decrease in the specific capacitance can be partially caused by the unstable electrochemical properties of the bare Ni-EP current collector at potentials higher than 0.5 V versus Ag/AgCl. For demonstrating this possibility, we investigated the electrochemical stability of bare Ni-EP (i.e., bare current collector) in 0.5 M Na<sub>2</sub>SO<sub>4</sub> electrolyte solution through repetitive CV scans. In this case, the

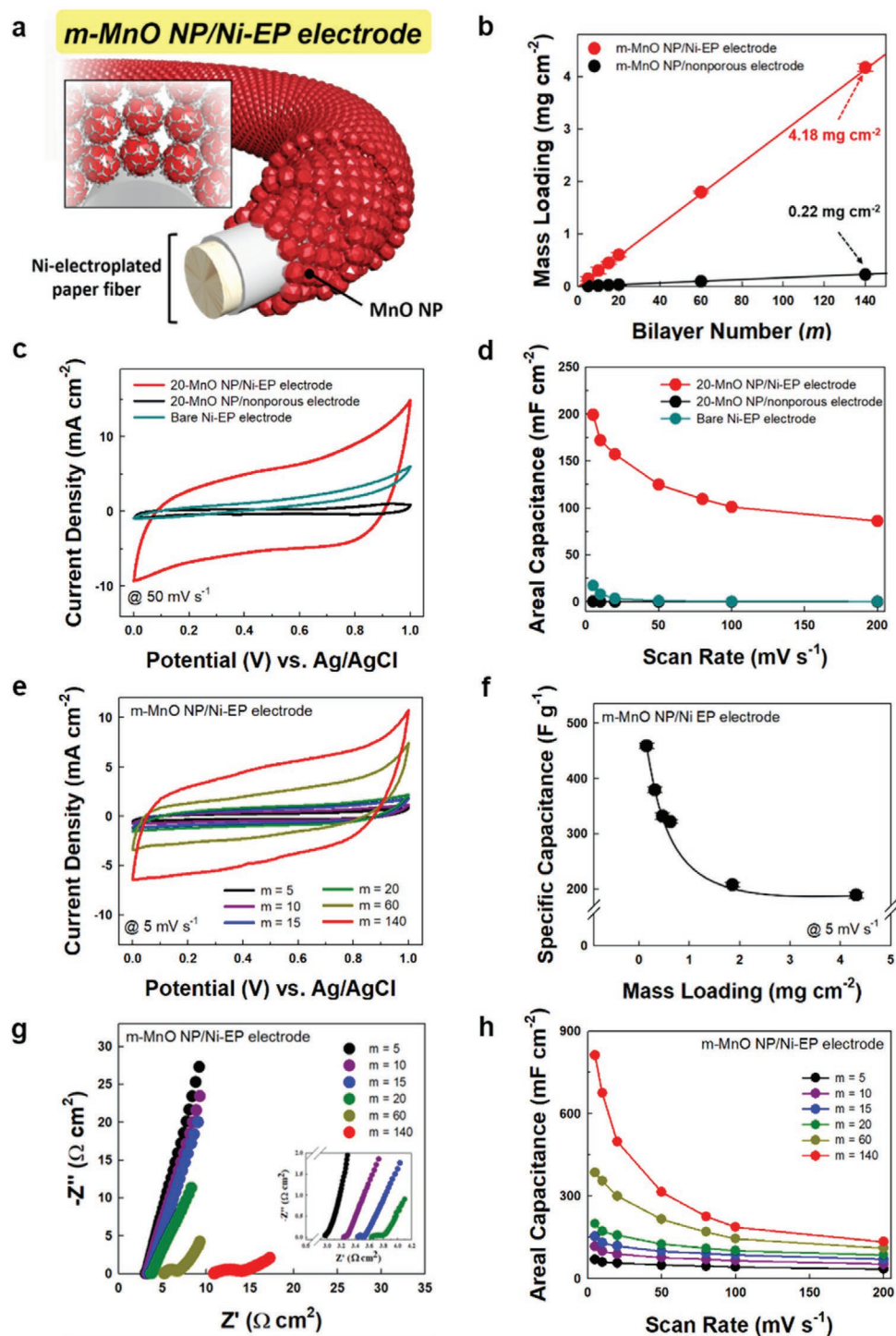


**Figure 5.** a) Schematic illustration of the *m*-MnO NP/Ni-EP electrodes. b) Mass loadings of the *m*-MnO NPs onto the Ni-EP and the nonporous electrode up to 140 bilayers. In this case, values of 0.15, 0.30, 0.45, 0.60, 1.80, and 4.18  $\text{mg cm}^{-2}$  for the mass loading of (OA-MnO NP/TREN)<sub>*m*</sub> multilayers correspond to *m* = 5, 10, 15, 20, 60, and 140 bilayers, respectively. c) Cyclic voltammograms of the 20-MnO NP/Ni-EP electrode, 20-MnO NP/nonporous electrode, and bare Ni-EP electrode at a scan rate of 50  $\text{mV s}^{-1}$ . d) Areal capacitance values of the 20-MnO NP/Ni-EP electrode, 20-MnO NP/nonporous electrode, and bare Ni-EP electrode as a function of scan rate. e) CVs of the *m*-MnO NP/Ni-EP electrode as a function of bilayer number of (OA-MnO NP/TREN)<sub>*m*</sub> multilayers at a scan rate of 5  $\text{mV s}^{-1}$ . f) Specific capacitance values of the *m*-MnO NP/Ni-EP electrode as a function of the mass loading of MnO NPs at 5  $\text{mV s}^{-1}$ . g) Nyquist plots of the *m*-MnO NP/Ni-EP electrode as a function of bilayer number of (OA-MnO NP/TREN)<sub>*m*</sub> multilayers in the frequency range of 0.1 Hz–100 kHz, measured at 0.1 V (amplitude potential ≈ 5 mV). h) Areal capacitance values of *m*-MnO NP/Ni-EP electrodes as a function of scan rate.

bare Ni-EP current collector exhibited an increase in the current density level and the integrated CV area by slight electro-oxidation of the electroplated Ni layer during repetitive CV scans. However, such an increase in the CV curve area of bare Ni-EP was negligible compared to that of 20-MnO NP/Ni-EP electrode (Figure S22, Supporting Information). Additionally, the bare Ni-EP current collector still exhibited an extremely low sheet resistance value below  $0.1 \Omega \text{ sq}^{-1}$  (initial sheet resistance  $\approx 0.08 \Omega \text{ sq}^{-1}$ ) after the 1000th cycle.

Although TREN, a small-molecule linker, can minimize the separation distance between vertically adjacent MnO NPs by removing bulky OA ligands, the poor electrical conductivity of MnO NPs themselves restricts the effective charge transfer between the current collector and the MnO NPs and between neighboring MnO NPs. Therefore, despite the intrinsically low conductivity of MnO NPs, it is reasonable to conclude that metallic fibril-based textiles with 3D porous structures contribute to an improvement in charge transfer within the Ni-EP-based electrode.

To further enhance the charge transfer within *m*-MnO NP multilayers, TOA-Au NPs were periodically incorporated into the *m*-MnO NP multilayers [i.e., (OA-MnO NP/TREN/TOA-Au NP/TREN)<sub>*m*</sub>] (Figure 6a). The bulky TOA ligands of TOA-Au are replaced by TREN linkers through the ligand exchange reaction, thus minimizing the amount of unnecessary insulating organic molecules in the multilayer electrodes.<sup>[13,41,45]</sup> Figure 6b shows the CV scans of the 140-MnO NP/Ni-EP electrodes with and without Au NP layers. The integrated CV area of the Au NP-incorporated electrode was 2.1 times larger than that of the electrode without Au NP layers, indicating significantly enhanced capacitance with the aid of metal NP layers. The Au NP-incorporated electrode exhibited a low  $R_s$  of  $3.6 \Omega \text{ cm}^2$  and  $R_{ct}$  of  $1.1 \Omega \text{ cm}^2$  despite the increased thickness of the multilayers, which were much less than those ( $R_s \approx 10.9 \Omega \text{ cm}^2$  and  $R_{ct} \approx 3.1 \Omega \text{ cm}^2$ ) of the electrode without Au NP layers (Figure 6c). These results show that the periodic incorporation of Au NPs into MnO NP multilayers can effectively enhance the charge transfer between neighboring MnO NP layers. With this improvement in charge transfer, the areal capacitance of the Au NP-incorporated MnO NP/Ni-EP electrode was  $1710 \text{ mF cm}^{-2}$  at a scan rate of  $5 \text{ mV s}^{-1}$ , which outperformed the areal capacitance of pseudocapacitive NP-based supercapacitor electrodes reported to date<sup>[13,50–54]</sup> as well as that of the 140-MnO NP/Ni-EP electrode without Au NP layers (Figure 6d). Additionally, the Au NP-incorporated electrode exhibited consistently higher capacitance values than the one without Au at scan rates ranging from 5 to  $200 \text{ mV s}^{-1}$ . We confirmed that the Au-incorporated MnO NP/Ni-EP electrode maintained 86.1% of its initial capacitance after 5000 CV cycles at  $100 \text{ mV s}^{-1}$  (Figure 6e), which implies robust and stable adsorption of the MnO NPs. To further confirm these phenomena, we investigated the electrochemical performance of Au NP-incorporated 60-MnO NP/Ni-EP with increasing current density from 2 ( $1.1 \text{ A g}^{-1}$ ) to  $20 \text{ mA cm}^{-2}$  ( $10.8 \text{ A g}^{-1}$ ) (Figure S23, Supporting Information). In this case, the electrochemical performance of Au NP-incorporated 60-MnO NP/Ni-EP was significantly enhanced compared to that of 60-MnO NP/Ni-EP without Au NP layers. Particularly, Au NP-incorporated 60-MnO NP/Ni-EP electrode exhibited good cycling stability by maintaining 95.2% of its initial capacitance even after 1000 cycles at a current density of  $10 \text{ mA cm}^{-2}$  ( $5.4 \text{ A g}^{-1}$ ) (Figure S24, Supporting Information).

Although *m*-MnO NP/Ni-EP electrode with Au NP layers exhibited a high areal capacitance at low scan rates due to conductive Au NPs, an extremely high loading amount of MnO NPs with poor electrical conductivity inevitably induced a dramatic decrease of areal capacitance at high scan rates. However, we highlight that a variety of active/conductive materials can be easily incorporated into our metallic paper-based current collector. Therefore, the electrochemical performance of the MnO NP-based electrodes used in this study can be further improved through the introduction of multilayers composed of carboxylic acid-functionalized multi-walled carbon nanotubes (i.e., COOH-MWCNTs) through LbL assembly (Figure S25, Supporting Information). As shown in Figure S25, 10-MnO NP-MWCNT/Ni-EP with Au NP layers and 10-MnO NP/Ni-EP with Au NP layers exhibited areal capacitances of 437 and  $70 \text{ mF cm}^{-2}$ , respectively at  $2 \text{ mA cm}^{-2}$ . Also, both electrodes showed  $\approx 80\%$  of Coulombic efficiency.

Furthermore, solid-state asymmetric supercapacitor (i.e., ASC) composed of 20-MnO NP/Ni-EP (positive electrode) and 20-Fe<sub>3</sub>O<sub>4</sub> NP/Ni-EP (negative electrode) using solid (i.e., Na<sub>2</sub>SO<sub>4</sub>/poly(vinyl alcohol) [PVA]) electrolytes was prepared and investigated. (Figure S27, Supporting Information). For this study, OA-Fe<sub>3</sub>O<sub>4</sub> NPs with a diameter of  $\approx 8 \text{ nm}$  were prepared, which have also a high affinity with amine groups of TREN. Therefore, all the experimental processes for the preparation of 20-Fe<sub>3</sub>O<sub>4</sub> NP/Ni-EP were exactly identical to those for 20-MnO NP/Ni-EP and characterized through CV measurements. The solid-state ASCs measured at a scan rate of  $50 \text{ mV s}^{-1}$  displayed CV curves with typical capacitive characteristics, suggesting the Faradaic reaction of the pseudocapacitive NPs within porous Ni-EP current collectors. Furthermore, we confirmed that this ASC could also display excellent mechanical and electrochemical stability under external stimuli conditions. This stable storage behavior was also observed during GCD measurements. The areal capacitances and Coulombic efficiencies of ASC were calculated from GCD profiles with different current densities of 2– $10 \text{ mA cm}^{-2}$ . The areal capacitances based on the total active materials containing both positive and negative electrodes ( $1.02 \text{ mg cm}^{-2}$ ) were measured to be  $\approx 68.8 \text{ mF cm}^{-2}$  for the solid-state ASC at a current density of  $2 \text{ mA cm}^{-2}$  ( $1.96 \text{ A g}^{-1}$ ). Considering that the better energy storage performance of our supercapacitor devices can be realized by active materials with more excellent electrochemical performance, our approach using LbL assembly-induced electroplating can provide a basis for developing a high-performance supercapacitor device through a current collector/energy reservoir with high electrical conductivity and large surface area.

### 3. Conclusion

We demonstrated that highly flexible papers and textiles with bulk metal-like conductivity and large surface areas could be prepared by a metal NP assembly-induced electroplating approach. After ligand exchange LbL assembly of Au NPs and extremely small-molecule linkers (i.e., TREN) on the insulating substrates, a minimal electrical conductivity ( $>10^{-5} \text{ S cm}^{-1}$ ) was achieved for metal electroplating with four multilayers. The subsequent Ni electroplating process transformed the metal

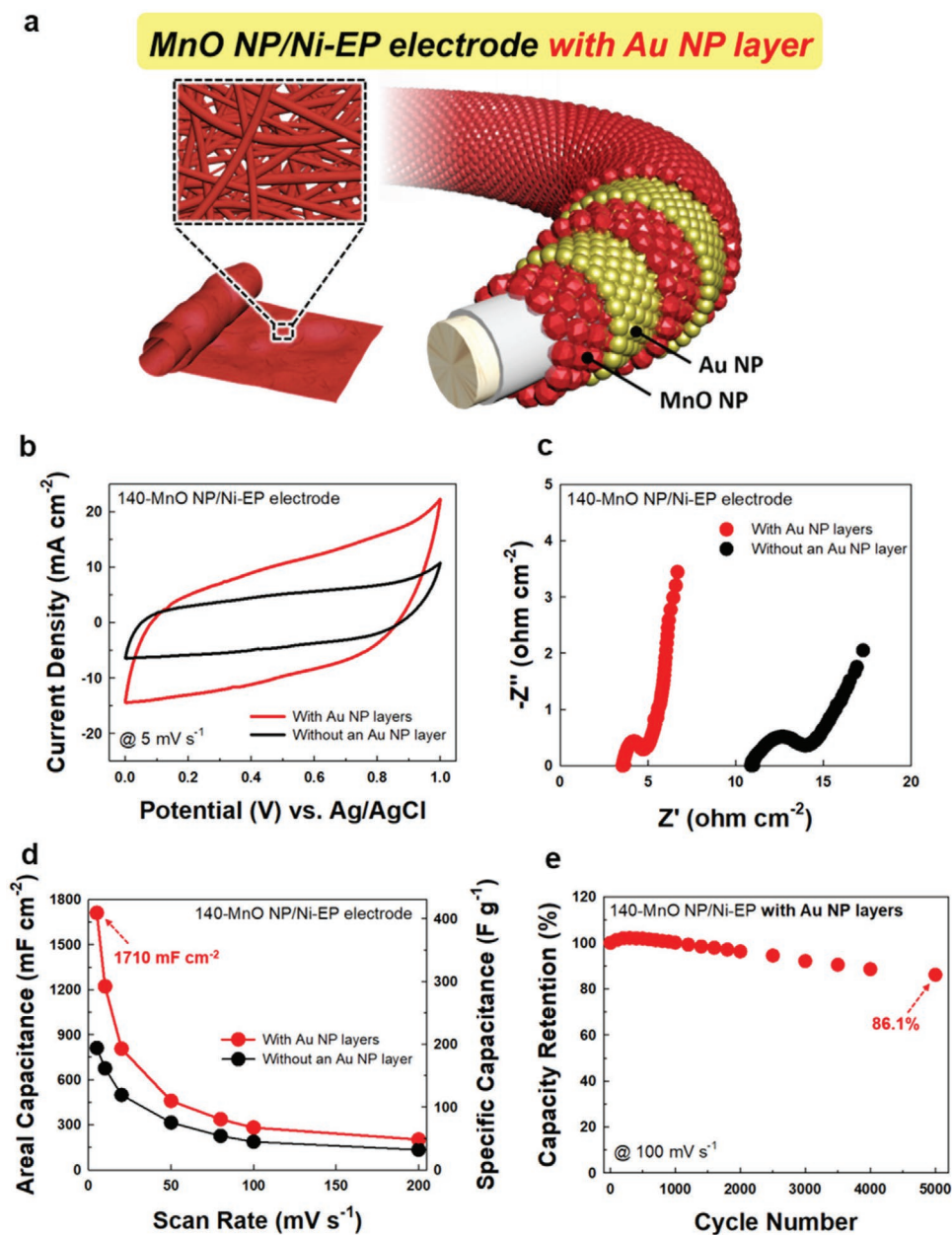


**Figure 6.** a) Schematic illustration of the m-MnO NP/Ni-EP electrodes with periodic Au NP layers. b) CVs of the 140-MnO NP/Ni-EP electrodes with and without Au NP layer at a scan rate of 5 mV s<sup>-1</sup>. c) Nyquist plots of the 140-MnO NP/Ni-EP electrodes with and without an Au NP layer in the frequency range of 0.1 Hz–100 kHz, measured at 0.1 V (amplitude potential ≈ 5 mV). d) Areal and specific capacitance values of the 140-MnO NP/Ni-EP electrodes with and without Au NP layer as a function of scan rate. e) Cycling retention of the capacitance of 140-MnO NP/Ni-EP electrodes with Au NP layer with a MnO NP mass loading of 4.18 mg cm<sup>-2</sup> at a scan rate of 100 mV s<sup>-1</sup>.

NP-assembled paper with relatively low electrical conductivity into highly conductive metallic paper (sheet resistance <0.1 Ω sq<sup>-1</sup>), which could be further improved through control of the electroplating conditions (i.e., external current flow, electroplating time, and number of pre-deposited metal NPs). We also demonstrated the efficiency and scalability of this process with various other metals, such as Au, Ag, and Cu. In addition to the cellulose papers, this electroplating method was also applied to various textile substrates, including polyesters, nylons, and cotton. Therefore, commercial metal

electroplating based on the two-electrode system could be fully applied to insulating paper or textile substrates with the help of ligand exchange LbL assembly. Furthermore, we confirmed that highly porous Ni-EPs with large surface areas could be used as conductive energy reservoirs for high-performance energy storage electrodes by further coating them with layers of MnO NPs. The (OA-MnO NP/TREN)<sub>20</sub> multilayer-coated Ni paper electrode exhibited a high areal capacitance of 199 mF cm<sup>-2</sup> (321 F g<sup>-1</sup>) at 5 mV s<sup>-1</sup>, which was 15 times higher than that of the nonporous electrode. The maximum areal capacitance

of MnO/Ni paper electrodes was found to be  $811 \text{ mF cm}^{-2}$  at a high MnO NP mass loading of  $4.31 \text{ mg cm}^{-2}$ . With the insertion of conductive Au NP layers among the MnO NP layers, the areal capacitance increased to  $1710 \text{ mF cm}^{-2}$ . Although our research motivation is to prepare the high-performance 3D porous current collectors as well as the high-performance supercapacitor electrodes through control of interfacial interactions such as electroplating, ligand exchange reaction, and insertion of conductive metal NPs, we highlight that a variety of electrochemically active materials such as CNTs, conductive polymers, and/or pseudocapacitive nanomaterials can be incorporated into our 3D porous Ni-EP current collectors using the previously reported approaches (a doctor blade, simple physical soaking, spraying, the Meyer rod coating process, and electrodeposition). We believe that our novel strategy that combines LbL assembly and commercial electroplating can provide an important and facile tool for flexible electrodes requiring a large specific area and bulk metal-like conductivity for various electrochemical applications, including energy storage electrodes.

#### 4. Experimental Section

**Synthesis of Hydrophobic NPs:** TOA-Au NPs with a diameter of  $\approx 8 \text{ nm}$  in toluene were synthesized through a two-phase reaction, which had been reported as the Brust method.<sup>[55]</sup> Briefly, 20 mm TOABr (Sigma-Aldrich) dispersed in toluene (80 mL) was vigorously mixed with 30 mm gold chloride trihydrate ( $\text{HAuCl}_4 \cdot 3\text{H}_2\text{O}$ , Sigma-Aldrich) in deionized water (30 mL). Then, a 0.4 M aqueous solution of  $\text{NaBH}_4$  (25 mL, Sigma-Aldrich) was added to the mixture as a reducing agent. The toluene phase containing TOA-Au NPs was separated from the aqueous solution, which was discarded. For removing residual reactants, the toluene solution was washed with  $\text{H}_2\text{SO}_4$  (0.1 M, 95% purity, Daejung Chemicals), NaOH (0.1 M, 97%, Sigma-Aldrich), and deionized water several times.

TOA-Ag NPs with a diameter of  $\approx 8 \text{ nm}$  in toluene were prepared by the modified Brust–Schiffrin method. In brief, 0.9 mmol of silver nitrate ( $\text{AgNO}_3$ ) in water (24 mL) and 2.25 mmol of TOABr in toluene (24 mL) were added to the flask and stirred for 10 min at  $25^\circ\text{C}$ . When sodium thiosulfate ( $\text{Na}_2\text{S}_2\text{O}_3$ ) (3.6 mmol) was added to the mixture, the cloudy mixture solution was turned to be clear. After 10 min, the transparent toluene phase containing silver precursor ions ( $\text{Ag}^+$ ) was transferred to another reaction flask. Next, 1.35 mmol of  $\text{NaBH}_4$  in deionized water (24 mL) was added to the toluene solution. The mixture solution was vigorously stirred for 10 min. After that, the deep brown-colored toluene phase was separated from the mixture solution, and consecutively washed with water, HCl (10 mM), and NaOH (10 mM) using a separating funnel. After that, the TOA-Ag NPs with  $\approx 8 \text{ nm}$  in diameter was obtained.

TOA-Cu NPs with a diameter of  $\approx 8.5 \text{ nm}$  dispersed in toluene were synthesized according to the modified Brust–Schiffrin method. Briefly, 0.75 mm of TOABr in toluene (8 mL) were vigorously stirred with 0.3 mm of copper (II) chloride dehydrate ( $\text{CuCl}_2 \cdot 2\text{H}_2\text{O}$ ) in deionized water (7 mL) and 1.2 mm of  $\text{Na}_2\text{S}_2\text{O}_3$  was consecutively poured into the solution. Then, 0.9 mm of  $\text{NaBH}_4$  in deionized water (1 mL) was added to the mixture. After 10 min, the toluene phase, separated from the mixture, was washed with 0.01 M HCl, 0.01 M  $\text{NH}_4\text{OH}$ , and deionized water.

OA-MnO NPs, with diameters of  $\approx 7 \text{ nm}$ , were synthesized according to a previous report.<sup>[56]</sup> A Mn-oleate precursor complex was initially prepared by the thermal reaction from a mixture of chloride tetrahydrate ( $\text{MnCl}_2 \cdot 4\text{H}_2\text{O}$ , Sigma-Aldrich), sodium oleate (97%, TCI Co., Ltd), ethanol, *n*-hexane, and deionized water at  $70^\circ\text{C}$  for 12 h. The mixture of the obtained red-colored Mn-oleate powder (1.24 g) and 1-hexadecene (12.8 mL) was stirred at  $70^\circ\text{C}$  for 1 h. The mixture was then heated from

70 to  $280^\circ\text{C}$  at a rate of  $2^\circ\text{C min}^{-1}$  under an argon atmosphere and maintained for 10 min. The formed OA-MnO NPs were separated from the resultant mixture including excess OA ligands through the addition of acetone as a poor solvent and the subsequent centrifugation. After that, the hydrophobic OA-MnO NPs were re-dispersed and kept in toluene or hexane.

OA- $\text{Fe}_3\text{O}_4$  NPs with diameters of  $\approx 8 \text{ nm}$  were synthesized in toluene as reported by Sun et al.<sup>[57]</sup>  $\text{Fe}(\text{acac})_3$  (2 mmol), 1,2-hexadecanediol (10 mmol), oleylamine (6 mmol), OA (5 mmol), and benzyl ether (20 mL) were mixed under nitrogen. The solution mixture was heated to  $200^\circ\text{C}$  for 2 h and then refluxed ( $300^\circ\text{C}$ ) for 1 h under nitrogen. The resulting black-colored solution was cooled to room temperature. Next, 40 mL of ethanol was added to the solution, and the resulting black product was separated using centrifugation. The product was dissolved in toluene in the presence of OA (0.05 mL) and oleylamine (0.05 mL). Centrifugation (6000 rpm, 10 min) was further applied to remove residues. A black-brown toluene dispersion of 8-nm-sized OA- $\text{Fe}_3\text{O}_4$  NPs was produced.

**Synthesis of COOH-MWCNTs:** Pristine MWCNTs were oxidized by strong acid treatment with  $\text{H}_2\text{SO}_4/\text{HNO}_3$  at  $70^\circ\text{C}$  for 3 h. Then, the carboxylic acid-functionalized MWCNTs (i.e., COOH-MWCNT) were purified with deionized water. Finally, the COOH-MWCNT film was obtained from vacuum filtration process, which was re-dispersed in ethanol. The resultant solution was diluted to  $5 \text{ mg mL}^{-1}$ .

**LbL-Assembled Metal NPs onto Papers and Textiles:** Hydrophobic metal NPs (TOA-Au, TOA-Ag, and TOA-Cu NPs) in toluene ( $5 \text{ mg mL}^{-1}$ ) and TREN ( $M_w \approx 146 \text{ g mol}^{-1}$ ) in ethanol ( $1 \text{ mg mL}^{-1}$ ) were deposited alternately onto a commercial paper substrate using an LbL assembly. First, the substrate was dipped into a TREN solution for 10 min and washed with pure ethanol to eliminate weakly bonded TREN molecules. Second, the TREN-coated substrate was dipped into the hydrophobic metal NP solution for 30 min and washed with pure toluene, resulting in one bilayer film. These procedures were repeated for preparing the conductive substrate with the sufficient electrical conductivity that could be electroplated. Although the loading amount of TOA-Au NPs onto the substrates could be controlled by the various methods such as solution concentration, dipping time, and bilayer number, we controlled only the bilayer number ( $n$ ) of (TOA-Au NP/TREN) $_n$  multilayers at the fixed solution concentration ( $5 \text{ mg mL}^{-1}$  for TOA-Au NP and  $1 \text{ mg mL}^{-1}$  for TREN) and deposition time (30 min for TOA-Au NP and 10 min for TREN).

**Preparation of Electroplated Paper and Textiles:** For the preparation of Ni-electroplated paper or textiles, the electrolyte solution (Watts bath) was prepared using  $240 \text{ g L}^{-1}$  nickel(II) sulfate hexahydrate ( $\text{NiSO}_4 \cdot 6\text{H}_2\text{O}$ , Sigma-Aldrich),  $45 \text{ g L}^{-1}$  nickel(II) chloride hexahydrate ( $\text{NiCl}_2 \cdot 6\text{H}_2\text{O}$ , Sigma-Aldrich),  $30 \text{ g L}^{-1}$  boric acid ( $\text{H}_3\text{BO}_3$ , Sigma-Aldrich), and deionized water.<sup>[58–61]</sup> Then, the process of Ni electroplating based on two electrode system was performed on the (TOA-Au NP/TREN) $_4$ -coated substrate as a cathode and a Ni foil as an anode that were connected to the power supply (see Figure S6, Supporting Information). After that, Ni-electroplated substrates were rinsed with pure water, and then dried using air stream. In the case of Ag-electroplated textile, the electrolyte solution was prepared using the mixture containing  $34 \text{ g L}^{-1}$  silver nitrate ( $\text{AgNO}_3$ , Sigma-Aldrich),  $6 \text{ g L}^{-1}$  nitric acid ( $\text{HNO}_3$ , Sigma-Aldrich),  $3 \text{ g L}^{-1}$  citric acid ( $\text{C}_6\text{H}_8\text{O}_7$ , Sigma-Aldrich), and deionized water. After that, Ag-electroplating process was carried out using the abovementioned process. Additionally, Cu-electroplated textile was prepared using the electrolyte solution containing  $1000 \text{ g L}^{-1}$  copper (II) sulfate pentahydrate ( $\text{CuSO}_4 \cdot 5\text{H}_2\text{O}$ , Sigma-Aldrich),  $50 \text{ g L}^{-1}$  sulfuric acid ( $\text{H}_2\text{SO}_4$ , Sigma-Aldrich), and deionized water. The Cu-electroplating process was carried out using the same electroplating conditions as those for Ni-electroplating. For Au-electroplated textile, the electroplating solution of  $25 \text{ mm}$  gold (III) chloride trihydrate ( $\text{HAuCl}_4$ , Sigma-Aldrich),  $0.3 \text{ M}$  5,5'-dimethylhydantoin (DMH, Sigma-Aldrich),  $0.36 \text{ M}$  potassium carbonate ( $\text{K}_2\text{CO}_3$ , Sigma-Aldrich),  $30 \text{ mg L}^{-1}$  polyethylenimine (PEI, Sigma-Aldrich), and deionized water. Subsequent electroplating process is identical to Ni-electroplating.

**Preparation of Ni-Electroless Deposited Paper:** For the preparation of electroless Ni-deposited paper or textile, the substrate was first immersed into a solution containing 37% HCl and 26 mM tin chloride (SnCl<sub>2</sub>) for 10 min.<sup>[48]</sup> Then, the substrate was dipped into the activating solution composed of 1.7 mM palladium chloride (PdCl<sub>2</sub>), 37% HCl, 0.32 M boric acid (H<sub>3</sub>BO<sub>3</sub>), and then rinsed with deionized water. Finally, the Ni was electroless-deposited onto the activated substrate by immersing into the nickel plating solution composed of 30 or 6 mM nickel sulfate hexahydrate (NiSO<sub>4</sub>·6H<sub>2</sub>O), 27 mM trisodium citrate dihydrate (Na<sub>3</sub>C<sub>6</sub>H<sub>5</sub>O<sub>7</sub>·2H<sub>2</sub>O), 0.34 M ammonium chloride (NH<sub>4</sub>Cl), and 0.14 M sodium hypophosphite (NaH<sub>2</sub>PO<sub>2</sub>·H<sub>2</sub>O). All reagents were purchased from Sigma-Aldrich.

**Preparation of Supercapacitor Electrodes:** For the preparation of m-MnO NP/Ni-EP electrodes, OA-MnO NPs in toluene (5 mg mL<sup>-1</sup>) and TREN in ethanol (1 mg mL<sup>-1</sup>) were deposited onto the Ni-EP substrates using a ligand exchange reaction-induced LbL assembly with a dipping time of 10 min per each component and washing process (toluene washing after the deposition of OA-MnO NPs and ethanol washing after the deposition of TREN). These processes were repeated until the desired bilayer number, and then the formed supercapacitor electrodes were dried using air stream.

For the preparation of m-MnO NP/Ni-EP electrodes with Au NP layers, OA-MnO NPs in toluene (5 mg mL<sup>-1</sup>), TREN in ethanol (1 mg mL<sup>-1</sup>), TOA-Au NPs (5 mg mL<sup>-1</sup>) in toluene, and TREN in ethanol (1 mg mL<sup>-1</sup>) were successively deposited onto the Ni-EP substrates using the abovementioned same LbL assembly and deposition conditions. These processes were also repeated until the desired bilayer number, and then the formed supercapacitor electrodes were dried using air stream.

For the preparation of 10-MnO NP-MWCNT/Ni-EP electrode with Au NP layers, the COOH-MWCNT in ethanol (5 mg mL<sup>-1</sup>) and TREN in ethanol (1 mg mL<sup>-1</sup>) were first subsequently deposited onto the Ni-EP substrates using a hydrogen-bonding reaction-induced LbL assembly. These processes were repeated until ten bilayers for the preparation of (COOH-MWCNT/TREN)<sub>10</sub> multilayer-coated Ni-EP. After ten bilayers, OA-MnO NPs in toluene (5 mg mL<sup>-1</sup>), TREN in ethanol (1 mg mL<sup>-1</sup>), TOA-Au NPs (5 mg mL<sup>-1</sup>) in toluene, and TREN in ethanol (1 mg mL<sup>-1</sup>) were successively deposited onto the (COOH-MWCNT/TREN)<sub>10</sub> multilayer-coated Ni-EP substrate through ligand exchange reaction-induced LbL assembly. Dipping time for each component was fixed at 10 min. Finally, the formed supercapacitor electrode was dried using an air stream.

For the preparation of MnO<sub>2</sub>-electrodeposited Ni-EP, the as-prepared Ni-EP (1 cm × 4 cm) was first cleaned with ethanol and deionized water. The electrodeposition of MnO<sub>2</sub> was conducted in a three-electrode configuration which an Ag/AgCl (3 M NaCl) electrode, a Pt coil electrode, and the Ni-EP were connected as the reference, counter, and working electrode, respectively in an aqueous solution composed of 0.1 M manganese acetate tetrahydrate ((CH<sub>3</sub>COO)<sub>2</sub>Mn·4H<sub>2</sub>O) and 0.1 M Na<sub>2</sub>SO<sub>4</sub>. The electrodeposition process was carried out at a constant potential of -1.6 V for different periods of time from 30 to 800 s to control the amount of the MnO<sub>2</sub> deposited. After the deposition, the electrode was washed with deionized water and dried at ambient temperature. The mass loading of MnO<sub>2</sub> was measured by high-precision balance (KERN & SOHN GmbH) with a sensitivity of 0.01 mg.

For the solid-state ASC, PVA (Sigma-Aldrich)/Na<sub>2</sub>SO<sub>4</sub> polymer gel was used as both the separator and electrolyte. First, 0.5 M Na<sub>2</sub>SO<sub>4</sub> and 6 g of PVA were mixed with 60 mL water at 90 °C for 1 h. When the Na<sub>2</sub>SO<sub>4</sub>/PVA gel became clear, the as-prepared positive and negative electrodes were immersed for 1 h, then dried under vacuum for 30 min. After these processes, the electrodes were assembled facing each other.

## Supporting Information

Supporting Information is available from the Wiley Online Library or from the author.

## Acknowledgements

S.W., D.N., W.C. contributed equally to this work. This work was supported by a National Research Foundation of Korea (NRF) grant funded by the Korea government (2019R1A4A1027627, 2021R1A2C3004151).

## Conflict of Interest

The authors declare no conflict of interest.

## Data Availability Statement

Research data are not shared.

## Keywords

electrodeposition, layer-by-layer assembly, metal NP incorporation, metallic paper, textile supercapacitor electrodes

Received: January 17, 2021

Revised: February 24, 2021

Published online: March 18, 2021

- [1] M. Armand, J. M. Tarascon, *Nature* **2008**, 451, 652.
- [2] B. Wang, B. Luo, X. L. Li, L. J. Zhi, *Mater. Today* **2012**, 15, 544.
- [3] Y. Shao, M. F. El-Kady, L. J. Wang, Q. Zhang, Y. Li, H. Wang, M. F. Mousavi, R. B. Kaner, *Chem. Soc. Rev.* **2015**, 44, 3639.
- [4] Y. Ko, M. Kwon, Y. Song, S. W. Lee, J. Cho, *Adv. Funct. Mater.* **2018**, 28, 1804926.
- [5] K. Jost, C. R. Perez, J. K. McDonough, V. Presser, M. Heon, G. Dion, Y. Gogotsi, *Energy Environ. Sci.* **2011**, 4, 5060.
- [6] A. Levitt, D. Hegh, P. Phillips, S. Uzun, M. Anayee, J. M. Razal, Y. Gogotsi, *Mater. Today* **2020**, 34, 17.
- [7] Y. Zhu, M. Yang, Q. Huang, D. Wang, R. Yu, J. Wang, Z. Zheng, D. Wang, *Adv. Mater.* **2020**, 32, 1906205.
- [8] L. Hu, F. L. Mantia, H. Wu, X. Xie, J. McDonough, M. Pasta, Y. Cui, *Adv. Mater.* **2011**, 1, 1012.
- [9] C. Hwang, W.-J. Song, J.-G. Han, S. Bae, G. Song, N.-S. Choi, S. Park, H.-K. Song, *Adv. Mater.* **2018**, 30, 1705445.
- [10] F. Yi, H. Ren, J. Shan, X. Sun, D. Wei, Z. Liu, *Chem. Soc. Rev.* **2018**, 47, 3152.
- [11] C. H. Kwon, Y. Ko, D. Shin, M. Kwon, J. Park, W. K. Bae, S. W. Lee, J. Cho, *Nat. Commun.* **2018**, 9, 4479.
- [12] K. Jost, G. Diona, Y. Gogotsi, *J. Mater. Chem. A* **2014**, 2, 10776.
- [13] Y. Ko, M. Kwon, W. K. Bae, B. Lee, S. W. Lee, J. Cho, *Nat. Commun.* **2017**, 8, 536.
- [14] Y. Huang, M. Zhu, Y. Huang, Z. Pei, H. Li, Z. Wang, Q. Xue, C. Zhi, *Adv. Mater.* **2016**, 28, 8344.
- [15] L. Liu, Z. Niu, L. Zhang, W. Zhou, X. Chen, S. Xie, *Adv. Mater.* **2014**, 26, 4855.
- [16] B. Yao, J. Zhang, T. Kou, Y. Song, T. Liu, Y. Li, *Adv. Sci.* **2017**, 4, 1700107.
- [17] Y. Zhang, Y. Wang, T. Cheng, W. Lai, H. Pang, W. Huang, *Chem. Soc. Rev.* **2015**, 44, 5181.
- [18] W. Zhao, T. Chen, W. Wang, B. Jin, J. Peng, S. Bi, M. Jiang, S. Liu, Q. Zhao, W. Huang, *Sci. Bull.* **2020**, 65, 1803.
- [19] J. Zhou, J. Yu, L. Shi, Z. Wang, H. Liu, B. Yang, C. Li, C. Zhu, J. Xu, *Small* **2018**, 14, 1803786.
- [20] L. Liu, Y. Yu, C. Yan, K. Li, Z. Zheng, *Nat. Commun.* **2015**, 6, 7260.

- [21] H. Zhang, H. Ning, J. Busbee, Z. Shen, C. Kiggins, Y. Hua, J. Eaves, J. Davis, T. Shi, Y. Shao, J. Zuo, X. Hong, Y. Chan, S. Wang, P. Wang, P. Sun, S. Xu, J. Liu, P. V. Braun, *Sci. Adv.* **2017**, *3*, e1602427.
- [22] Y. Chen, T. Zhou, Y. Liu, Z. Guo, *J. Mater. Chem. A* **2017**, *5*, 23476.
- [23] Y. Guo, M. T. Otley, M. Li, X. Zhang, S. K. Sinha, G. M. Treich, G. A. Sotzing, *ACS Appl. Mater. Interfaces* **2016**, *8*, 26998.
- [24] L. Hu, J. W. Choi, Y. Yang, S. Jeong, F. L. Mantia, L.-F. Cui, Y. Cui, *Proc. Natl. Acad. Sci. U. S. A.* **2009**, *106*, 21490.
- [25] N. Kurra, B. Ahmed, Y. Gogotsi, H. N. Alshareef, *Adv. Energy Mater.* **2016**, *6*, 1601372.
- [26] P. Chen, H. Chen, J. Qiu, C. Zhou, *Nano Res.* **2010**, *3*, 594.
- [27] H. Chen, S. Zhou, L. Wu, *ACS Appl. Mater. Interfaces* **2014**, *6*, 8621.
- [28] H. M. Lee, S.-Y. Choi, A. Jung, S. H. Ko, *Angew. Chem., Int. Ed.* **2013**, *52*, 7718.
- [29] G. Xiang, Y. Meng, G. Qu, J. Yin, B. Teng, Q. Wei, X. Xu, *Sci. Bull.* **2020**, *65*, 443.
- [30] K. Chen, R. Pathak, A. Gurung, K. M. Reza, N. Ghimire, J. Pokharel, A. Baniya, W. He, J. J. Wu, Q. Qiao, Y. Zhou, *J. Mater. Chem. A* **2020**, *8*, 1911.
- [31] J. W. Huh, H.-J. Jeon, C. W. Ahn, *Curr. Appl. Phys.* **2017**, *17*, 1401.
- [32] I. Karacan, L. Erzurumluoglu, *Fibers Polym.* **2015**, *16*, 1629.
- [33] T. Yin, Y. Wang, L. He, X. Gong, *Comp. Mater. Sci.* **2017**, *138*, 27.
- [34] G. Decher, *Science* **1997**, *277*, 1232.
- [35] S. S. Shiratori, M. F. Rubner, *Macromolecules* **2000**, *33*, 4213.
- [36] S. W. Lee, N. Yabuuchi, B. M. Gallant, S. Chen, B. S. Kim, P. T. Hammond, Y. Shao-Horn, *Nat. Nanotechnol.* **2010**, *5*, 531.
- [37] Y. Kim, J. Zhu, B. Yeom, M. D. Prima, X. Su, J. Kim, S. J. Yoo, C. Uher, N. A. Kotov, *Nature* **2013**, *500*, 59.
- [38] M. Park, Y. Kim, Y. Ko, S. Cheong, S. W. Ryu, J. Cho, *J. Am. Chem. Soc.* **2014**, *136*, 17213.
- [39] J. Schmitt, G. Decher, W. J. Dressick, S. L. Brandow, R. Gee, R. Shashidhar, J. M. Calvert, *Adv. Mater.* **1997**, *9*, 61.
- [40] S. Y. Kim, J. Hong, R. Kaviani, S. W. Lee, M. N. Hyder, Y. Shao-Horn, T. Hammond, *Energy Environ. Sci.* **2013**, *6*, 888.
- [41] Y. Ko, H. Baek, Y. Kim, M. Yoon, J. Cho, *ACS Nano* **2013**, *7*, 143.
- [42] D. Nam, Y. Heo, S. Cheong, Y. Ko, J. Cho, *Appl. Surf. Sci.* **2018**, *440*, 730.
- [43] D. Shin, C. H. Kwon, Y. Ko, B. Lee, S. W. Lee, J. Cho, *J. Mater. Chem. A* **2018**, *6*, 20421.
- [44] S. Kang, D. Nam, J. Choi, J. Ko, D. Kim, C. H. Kwon, J. Huh, J. Cho, *ACS Appl. Mater. Interfaces* **2019**, *11*, 12032.
- [45] S. Lee, Y. Song, Y. Ko, Y. Ko, J. Ko, C. H. Kwon, J. Huh, S.-W. Kim, B. Yeom, J. Cho, *Adv. Mater.* **2020**, *32*, 1906460.
- [46] Y. Song, D. Kim, S. Kang, Y. Ko, J. Ko, J. Huh, Y. Ko, S. W. Lee, J. Cho, *Adv. Funct. Mater.* **2019**, *29*, 1806584.
- [47] Y. Kim, J. Zhu, B. Yeom, M. D. Prima, X. Su, J. G. Kim, S. J. Yoo, C. Uher, N. A. Kotov, *Nature* **2013**, *500*, 59.
- [48] Y.-H. Lee, J.-S. Kim, J. Noh, I. Lee, H. J. Kim, S. Choi, J. Seo, S. Jeon, T.-S. Kim, J.-Y. Lee, J. W. Choi, *Nano Lett.* **2013**, *13*, 5753.
- [49] Y. Zhang, C. J. Sheehan, J. Zhai, G. Zou, H. Luo, J. Xiong, Y. T. Zhu, Q. X. Jia, *Adv. Mater.* **2010**, *22*, 3027.
- [50] M. Toupin, T. Brousse, D. Bélanger, *Chem. Mater.* **2004**, *16*, 3184.
- [51] H. Gao, F. Xiao, C. B. Ching, H. Duan, *ACS Appl. Mater. Interfaces* **2012**, *4*, 2801.
- [52] L. Hu, W. Chen, X. Xie, N. Liu, Y. Yang, H. Wu, Y. Yao, M. Pasta, H. N. Alshareef, Y. Cui, *ACS Nano* **2011**, *5*, 8904.
- [53] Y. He, W. Chen, X. Li, Z. Zhang, J. Fu, C. Zhao, E. Xie, *ACS Nano* **2012**, *7*, 174.
- [54] L. Yuan, X. Lu, X. Xiao, T. Zhai, J. Dai, F. Zhang, B. Hu, X. Wang, L. Gong, J. Chen, C. Hu, Y. Tong, J. Zhou, Z. L. Wang, *ACS Nano* **2012**, *6*, 656.
- [55] M. Brust, M. Walker, D. Bethell, D. J. Schiffrin, R. Whyman, *J. Chem. Soc. Chem. Commun.* **1994**, *0*, 801.
- [56] J. Park, K. An, Y. Hwang, J. Park, H. Noh, J. Kim, J. Park, N. Hwang, T. Hyeon, *Nat. Mater.* **2004**, *3*, 891.
- [57] S. Sun, H. Zeng, D. B. Robinson, S. Raoux, P. M. Rice, S. X. Wang, G. Li, *J. Am. Chem. Soc.* **2004**, *126*, 273.
- [58] K. Nielsch, F. Muller, A. Li, U. Gosele, *Adv. Mater.* **2000**, *12*, 582.
- [59] H. Alimadadi, A. B. Fanta, T. Kasama, M. A. J. Somers, K. Pantleon, *Surf. Coat. Technol.* **2016**, *299*, 1.
- [60] J. P. Hoare, *J. Electrochem. Soc.* **1986**, *133*, 2491.
- [61] O. P. Watts, *Trans. Am. Electrochem. Soc.* **1916**, *29*, 395.